HHS Public Access

Author manuscript

Nat Genet. Author manuscript; available in PMC 2017 May 21.

Published in final edited form as:

Nat Genet. 2017 January ; 49(1): 87–96. doi:10.1038/ng.3728.

Inactivation of Capicua drives cancer metastasis

Ross A. Okimoto[1,2], **Frank Breitenbuecher**[3], **Victor R. Olivas**[1], **Wei Wu**[1,2], **Beatrice Gini**[1,2], **Matan Hofree**[4,5], **Saurabh Asthana**[2], **Gorjan Hrustanovic**[2], **Jennifer Flanagan**[2], **Asmin Tulpule**[1,2], **Collin M. Blakely**[1,2], **Henry J. Haringsma**[6], **Andrew D. Simmons**[6], **Kyle Gowen**[7], **James Suh**[7], **Vincent A. Miller**[7], **Siraj Ali**[7], **Martin Schuler**[3,8], and **Trever G. Bivona**[1,2]

[1]Department of Medicine, University of California, San Francisco, San Francisco, CA

[2]Helen Diller Family Comprehensive Cancer Center, University of California, San Francisco, San Francisco, CA

[3]Department of Medical Oncology, West German Cancer Center, University Hospital Essen, Essen, Germany

[4]Broad Institute of MIT and Harvard, Cambridge, Massachusetts

[5]Dana-Farber Cancer Institute, Harvard Medical School, Boston, Massachusetts

[6]Clovis Oncology Inc., San Francisco, California

[7]Foundation Medicine, Cambridge, Massachusetts

[8]German Cancer Consortium (DKTK), Heidelberg, Germany

Abstract

Metastasis is the leading cause of death in lung cancer patients, yet the molecular effectors underlying tumor dissemination remain poorly defined. Through development of an *in vivo* spontaneous lung cancer metastasis model, we show that the developmentally-regulated transcriptional repressor Capicua (CIC) suppresses invasion and metastasis. CIC inactivation relieves repression of its effector ETV4, driving ETV4-mediated upregulation of MMP24 that is necessary and sufficient for metastasis. Loss of CIC, or increased levels of its effectors ETV4 and MMP24, is a biomarker of tumor progression and worse outcomes in lung and gastric cancer patients. Our findings uncover CIC as a conserved metastasis suppressor, revealing new anti-metastatic strategies to improve patient outcomes.

Correspondence to: Trever G. Bivona MD PhD (trever.bivona@ucsf.edu).

Accession codes

Datasets can be found in Gene Expression Omnibus. Accession code GSE74866.

Author contributions

R.A.O. designed and performed the experiments, analyzed the data, and wrote the manuscript. R.A.O., F.B., V.O., and B.G. performed *in vivo* studies. M.H. and W.W. performed TCGA analysis. K.G., J.S., V.A.M., S.A. provided lung cancer datasets. S.A., J.F., A.S. analyzed RNAseq and CNA. G.H., A.T., C.M.B., and M.S. provided clinical samples. T.G.B. directed the project, designed and analyzed experiments, and wrote the manuscript.

Introduction

Non-small cell lung cancer (NSCLC) is the leading cause of cancer mortality worldwide[1]. Metastasis accounts for >90% of NSCLC-related deaths, yet its molecular basis remains poorly defined[2]. Models to study metastasis have traditionally relied upon experimental metastasis assays that directly inoculate tumor cells into the circulation[3]. While informative, these assays are influenced by tumor site injection and capture the later phases of metastasis[3]. Further limiting progress is the paucity of genetically-engineered mouse models that rapidly develop spontaneous lung cancer metastasis[4]. Thus, the identification of genes necessary for tumor dissemination is hampered by the lack of tractable *in vivo* systems for rapid monitoring and functional dissection of spontaneous metastasis. We hypothesized that developing an orthotopic *in vivo* platform to monitor and mechanistically dissect NSCLC progression would reveal a novel molecular mediator of metastasis. Through coordinated use of this *in vivo* platform and analysis of human clinical specimens, we identified the transcriptional repressor *Capicua* (*CIC*) and its downstream effectors *ETV4* and *MMP24* as critical mediators, and clinical biomarkers, of lung and gastric adenocarcinoma progression and metastasis. Our findings establish a CIC-controlled metastatic cascade, and uncover new anti-metastatic strategies to improve clinical outcomes.

Results

An orthotopic *in vivo* lung cancer metastasis model identifies CIC as a mediator of spontaneous metastasis

The *in vivo* orthotopic NSCLC system uses bioluminescent (BLI)-based detection of implanted tumor cells and allows for direct visualization of primary tumor formation, circulatory tracking of tumor-derived cells, and development of macroscopic metastasis (Fig. 1a). We initially studied epidermal growth factor receptor (*EGFR*)-mutant lung adenocarcinoma (LA) because *EGFR*-mutant LA's with an epithelial-to-mesenchymal transition (EMT) can acquire hypermigratory properties *in vitro* that may reflect increased metastatic potential, concomitant with EGFR inhibitor resistance[5–7]. But whether the molecular changes associated with the EMT promote spontaneous metastasis and also underlie drug resistance is unclear. Reasoning that the *in vivo* system might provide insight into these questions, we used the existing *EGFR*-mutant LA system consisting of parental EGFR inhibitor (rociletinib)-sensitive H1975 epithelial cells and two mesenchymal drug-resistant sublines (H1975 M1 and M2, previously called H1975 COR 10-1 and COR 1-1, respectively) independently derived from the parental population through prolonged rociletinib exposure (Supplementary Fig. 1a)[6]. *In vitro* analyses revealed these M1 and M2 sublines were hyperinvasive and maintained rociletinib resistance upon drug washout, suggesting a stable molecular and phenotypic switch (Supplementary Fig. 1b–d).

Parental H1975 and H1975 M1 cells were engineered to express luciferase (Luc) and green fluorescent protein (GFP) and directly implanted into the left lung of immunocompromised (SCID) mice using a surgical transpleural approach[8–9]. Primary lung tumors were observed three days following implantation in ~70% of mice by BLI detection. Notably, 100% of H1975 M1-bearing mice developed mediastinal lymph node (LN) and contralateral lung metastasis within two weeks, compared to a 28% metastatic efficiency rate in the H1975

cohort (Fig. 1b–c). *Ex vivo* BLI detected Luc+ cells within the right (metastasis) and left (primary) lungs of H1975 M1 mice at five weeks post-implantation (Supplementary Fig. 1e). $EGFR^{L858R}$ immunohistochemistry (IHC) confirmed the presence of mutant EGFR expressing tumor-cells (Supplementary Fig. 1f–g). Whole blood was isolated from tumor-bearing mice and GFP+ circulating tumor cells (CTCs) were quantified by fluorescent-activated cell sorting. We observed a ~5-fold increase in GFP+ CTCs in the H1975 M1 cohort compared to H1975 mice (Fig. 1d). H1975 M1 cells did not have a growth advantage over H1975 cells *in vitro* or *in vivo* (Supplementary Fig. 1h–i), suggesting that tumor dissemination was not a consequence of increased proliferation. Our findings represent a rare demonstration of *in vivo* spontaneous lung cancer metastasis that recapitulates salient features of human NSCLC.

Restoring CIC suppresses lung cancer metastasis

To identify the molecular cause of increased metastatic potential in H1975 M1 cells, we performed whole exome sequencing (WES) mutational and copy number variation (CNV) analysis making comparison to H1975 cells. We identified an identical homozygous deletion at 19q13 in both H1975 M1 and M2 that was not detected in parental H1975 cells (Fig. 1e–f, Supplementary Fig. 2a–c). Three adjacent genes were deleted, *ERF, CIC*, and *PAFAH1B3* in H1975 M1 cells (Supplementary Fig. 3a–b). To test whether loss of these genes enhanced metastasis, we reconstituted *ERF, CIC*, and *PAFAH1B3* into hypermetastatic H1975 M1 cells and compared metastatic capacity using the *in vivo* system (Supplementary Fig. 3c–e). Only CIC rescue decreased metastasis (91%, 10/11 mice were metastasis-free), even compared to the parental H1975 cohort (75%, 3/4 mice metastasis-free) (Fig. 1g–h, Supplementary Fig. 3f–i). We also observed a reduction in GFP+ CTCs in CIC-rescue mice compared to control (Fig. 1i). Notably, the expression of reconstituted CIC in H1975 M1 cells was comparable to endogenous CIC in H1975 cells (Supplementary Fig. 3j). Single-cell analysis of parental H1975 cells, revealed a pre-existing subpopulation with homozygous *CIC* loss (~8%) (Supplementary Fig. 4a). Moreover, we found decreased CIC expression in metastatic tumors from the rare H1975 mice that developed metastasis when compared to primary tumors (Supplementary Fig. 4b–c). These findings suggest the selective outgrowth of pre-existing *CIC*-null cells from the H1975 bulk population that confer metastatic progression. Analysis of *in vivo* and *in vitro* growth rates demonstrated a slight growth disadvantage in CIC reconstituted tumors (Fig. 1j, Supplementary Fig. 5a), suggesting that CIC may regulate tumor growth in addition to metastasis. In concordance, a putative tumor suppressor role for CIC in oligodendroglioma (OG) and prostate cancer has been suggested and in drosophila intestinal stem cells CIC decreases proliferation through cell-cycle gene repression[10–13]. However, whether CIC suppresses metastasis is unknown.

We reasoned that if CIC loss confers increased metastatic potential, in addition to proliferation, then metastatic tumors might harbor more frequent genetic inactivation of CIC than non-metastatic tumors. We queried 488 patients in the TCGA LA dataset and found a CIC mutation rate of 0.5% in early (n = 381) and 2.8% in advanced-stage (n = 107) cases (Supplementary table 1). Additionally, we identified a 5.9% (2/34) *CIC* mutation rate in metastatic LA cases similarly examined by WES[14]. Collectively, these data establish a *CIC* mutation rate of 0.5% (2/381) in early stage (I–II) and 3.5% (5/141) in advanced-stage (III–

IV) LA patients (n=522, p=0.02) (Supplementary table 1). We next analyzed >1300 LA tumors from advanced-stage patients. This analysis revealed *CIC* alterations in 3.1% (42/1342) of patients, including truncations, insertions, and a genomic deletion (deleterious events) (Fig. 2a). These clinical data suggest that *CIC* mutations are enriched in tumors from advanced-stage LA patients, supporting a role for CIC in metastasis in addition to tumor proliferation.

We next engineered 11 *CIC* mutants selected from the advanced-stage cohort to functionally interrogate *in vitro* and *in vivo*. These CIC mutations were localized to the N-terminus (G107E, R181W), the DNA-binding domain (Q247R), the repressor domain (R1515H, Q1516H), and an uncharacterized region between the DNA-binding and repressor domains (A281S, S649F, R666C, P722L, G1098D, A1185T) (accession NC_000019.9). To assess the functional impact of these mutations on invasion, we expressed all 11 CIC mutants in H1975 M1 cells and performed *in vitro* trans-well assays (Fig. 2b, Supplementary Fig. 6a). All CIC mutants tested were loss-of-function with respect to invasive potential, as these mutants were unable to suppress the hyperinvasive phenotype relative WT CIC (Fig. 2c). We next tested select CIC mutants in the *orthotopic* model and found that each mutant failed to suppress the hypermetastatic phenotype of H1975 M1 cells compared to WT CIC (Fig. 2d–e). One mutant (G107E) exhibited a modest loss-of-function phenotype *in vitro* and *in vivo*, compared with the other mutants tested. These data establish the loss-of-function phenotype of several *CIC* mutations identified in advanced-stage LA.

CIC has no established role in LA progression or metastasis, but plays a crucial role in lung alveolarization, a developmental process regulated by ECM remodeling[15,16]. The mechanism by which CIC governs ECM maintenance may be through repression of the *ETV4* transcription factor that promotes the expression of MMPs (Fig. 2f)[15,17]. We hypothesized that CIC loss de-represses ETV4 to augment ECM remodeling genes including MMPs to promote invasion and metastasis (Fig. 3a). To explore this, we confirmed *ETV4* promoter occupancy by CIC with chromatin immunoprecipitation-PCR (ChIP-PCR) in both H1975 (endogenous CIC) and H1975 M1 (reconstituted CIC) cells (Fig. 3b, Supplementary Fig. 6b). Next, we confirmed de-repression of *ETV4* in H1975 M1 and M2 cells (Supplementary Fig. 6c). To identify CIC-ETV4 metastasis-specific targets, we performed comparative transcriptome analysis of H1975 M1 and CIC-reconstituted H1975 M1 cells (Supplementary table 2). While we observed CIC-responsive differential expression (DE) of cell cycle genes, we also observed enrichment in ECM remodeling genes (Supplementary Fig. 5b–c)[18]. We next compared the transcriptional profile of H1975 to H1975 M1 and M2 cells. Functional annotation (using DAVID) of the top 1000 DE genes between H1975 and each metastatic subline confirmed enrichment in proteinaceous ECM genes (Enrichment score (ES) = 8.36, p = 3.60e-10 for H1975 M1, ES = 5.67, p = 3.20e-06 for H1975 M2) (Supplementary table 3a–b). Independent GO analysis using GeneTrail, confirmed ECM gene enrichment (p = 1.63e-09 for H1975 M1, p = 4.02e-06 for H1975 M2). Thus, we hypothesized that CIC regulates metastasis through a downstream ECM remodeling program. In this way, CIC engages distinct downstream pathways to preferentially drive different phenotypic responses, such as proliferation or metastasis. We reasoned that the orthotopic model would allow for discovery and functional validation of the CIC-responsive gene(s) that selectively drives cancer metastasis, without directly impacting tumor growth.

CIC represses ETV4-mediated MMP24 expression in lung adenocarcinoma

To identify a CIC-regulated metastasis effector, we investigated whether individual genes present in the ECM cluster correlated with clinical outcomes, using publically-available mRNA datasets[19]. Of the 46 (H1975 M1) and 37 (H1975 M2) differentially expressed ECM genes in each subline, we selected the most highly upregulated genes shared between the two cell lines for analysis (*SLC1A3, WNT5A, HAPLN1, COL8A1, MMP24*; an *ADAMTS10* probe was not present) (Supplementary Fig. 6d). Of the five candidate genes only *MMP24* upregulation (increased 24-fold in H1975 M1; 11-fold in H1975 M2) was significantly associated with worse progression-free survival (PFS) in patients with LN-positive NSCLC (N1; N=130) (Fig. 3c, Supplemental Fig. 6e–h). A similar trend towards worse PFS in unselected NSCLC patient tumors expressing high MMP24 was observed (N=982, p-value 0.069) (Supplementary Fig. 6i). As worse PFS can reflect metastatic progression, the data indicate that increased MMP24 in NSCLC identifies patients at high-risk for tumor progression and worse outcome. We further investigated MMP24 expression in two tissue microarrays (TMAs) containing 32 paired primary LAs and matched LN metastasis. Basal MMP24 IHC staining was observed in primary tumors, and MMP24 expression was elevated upon metastasis in association with decreased CIC expression (Fig. 3d, Supplementary Fig 6j–l). Thus, the increased MMP24 present in H1975 M1 and M2 cells is significantly and specifically associated with tumor progression and worse clinical outcome.

To investigate whether CIC regulates MMP24 via ETV4, we knocked down (KD) *ETV4* in H1975 and H1975 M1 cells and observed decreased MMP24 levels (Supplementary Fig. 7a). We next identified three ETV4 binding elements (AGGAA) in the *MMP24* promoter (Supplementary Fig. 7b). ChIP-PCR in H1975 M1 cells revealed MMP24 promoter occupancy by ETV4 and promoter assays showed that ETV4 overexpression increased *MMP24* activity (Supplementary Fig. 6c–d), suggesting that ETV4 regulates *MMP24* expression. We next established stable CIC KD in H1975 cells using three independent hairpins (shCICa-c). CIC KD increased ETV4 and MMP24 (Fig. 3e), which enhanced metastatic efficiency compared to control (Fig. 3f–g). *Ex vivo* imaging confirmed contralateral metastasis in mice bearing CIC KD (Supplementary Fig. 7e). Thus, CIC loss is sufficient to promote LA metastasis. In contrast to CIC reconstitution, which suppressed H1975 M1 growth, we did not observe an increase in tumor growth with CIC KD (Supplementary Fig. 7f–g). These data suggest that different thresholds of CIC expression and transcriptional modulation of its target genes may regulate the distinct functional outputs that CIC controls.

In further support of this linked CIC-ETV4-MMP24 axis, CIC reconstitution in H1975 M1 cells decreased ETV4, MMP24, and invasion (Fig. 3h–i, Supplementary Fig. 7h). Decreased invasiveness was directly linked to MMP24, as MMP24 re-expression in CIC-expressing H1975 M1 cells rescued the invasive phenotype (Fig. 3i, Supplementary Fig. 71). Consistent with this, CIC-mediated suppression of H1975 M1 metastasis *in vivo* (Fig. 1g) was associated with decreased MMP24 tumor expression (Supplementary Fig. 7j–k). Interestingly, *CIC* re-expression failed to restore rociletinib sensitivity, suggesting that CIC

controls metastatic potential but not EGFR inhibitor sensitivity (Supplementary Fig. 7l). Thus, CIC regulates ETV4 and MMP24 to control metastatic capacity in LA.

MMP24 is a multistep effector of lung cancer metastasis

MMP24 is a membrane-type MMP with no role in metastasis, but it promotes neuronal migration[20]. We hypothesized that MMP24 is necessary and sufficient for lung cancer invasion and metastasis. We confirmed increased *MMP24* expression in H1975 M1 and M2 cells, then performed *MMP24* KD with two distinct shRNAs (shMMP24a, b) (Supplementary Fig. 8a–b). MMP24 silencing reduced invasion and metastasis, without impacting primary tumor implantation or growth (Fig. 4a–b, Supplementary Fig. 8c–h). CTCs were reduced in MMP24 KD mice compared to control (Fig. 4c). Further, MMP24 expression was localized to the leading edge of primary tumors in H1975 M1 mice, consistent with an invasive-driving function (Fig. 4d). Immunofluorescence using tumor-specific markers (GFP and human-specific vimentin) showed that these MMP24-expressing cells were tumor-derived (T) invading into mouse lung (L) (Fig. 4e). These data suggest that MMP24 confers invasive capacity to promote tumor dissemination from the primary site.

We next determined if MMP24 is sufficient to promote extravasation and colonization. We overexpressed MMP24 in weakly metastatic H1975 cells (Supplementary Fig. 8i), and assessed lung colonization using a tail vein assay[21]. Both H1975 and H1975 MMP24-overexpressing cells reached the pulmonary circulation at day one (Supplementary Fig. 8j–k). However, by day 21 pulmonary luminescence in the control mice was nearly undetectable (Supplementary Fig. 8k), indicating these cells were incapable of stable colonization. In contrast, pulmonary luminescence in mice harboring cells overexpressing MMP24 persisted throughout the 21-day period (Supplementary Fig. 8j–k). Thus, MMP24 promotes tumor-cell circulatory extravasation and stable lung colonization.

MMP24 was also sufficient for spontaneous metastasis, as MMP24 overexpression in H1975 cells increased invasion and promoted spontaneous tumor dissemination to metastatic sites, including bone, in the orthotopic system (Fig. 4f–i, Supplementary Fig. 8l–n). MMP24 overexpression did not confer a growth advantage in H1975 cells (Supplementary Fig. 8o). Thus, our *in vivo* molecular dissection identifies CIC and its downstream effector and ETV4 target, MMP24 as a multi-step mediator of metastasis and suggests that the functional effectors downstream of CIC that mediate metastasis or proliferation may be distinct.

MMP24 promotes metastasis across multiple NSCLC models

MMP24 overexpression did not confer rociletinib resistance in H1975 cells (Supplementary Fig. 9a), suggesting that CIC-mediated metastasis is uncoupled from EGFR inhibitor resistance. Thus, we examined whether MMP24 controls metastasis more broadly in LA. Assessment of baseline invasiveness in treatment-naive human LA cells revealed that A549 and HCC364 cells were highly invasive (Supplementary Fig. 9b). MMP24 silencing suppressed invasion in A549 and HCC364 cells (Supplementary Fig. 10a–b, h–i). Moreover, MMP24 KD was linked to reduced MMP24 proteolytic activity, as MMP24 silencing decreased N-Cadherin cleavage (known MMP24 substrate) in A549 cells (Supplementary

Fig. 9c), suggesting MMP24 may enhance peri-cellular invasion via proteolysis of adhesion proteins[22].

We employed the orthotopic system to assess whether MMP24 promotes metastasis in A549 and HCC364 cells. Whereas 100% of mice in the A549 and HCC364 control groups developed spontaneous metastasis within one week, MMP24 KD reduced metastasis without impacting growth (Fig. 4j–k, Supplementary Fig. 10c, j–l). Persistent MMP24 suppression and absence of luciferase activity in the contralateral lung of non-metastatic mice was confirmed by IHC and *ex vivo* BLI in A549 and HCC364 mice (Supplementary Fig. 10d–e, 10m–n). CTCs were reduced upon MMP24 silencing in A549 and HCC364 mice, most prominently in mice without metastasis (Supplementary Fig. 10f, 10o). In A549 and HCC364 MMP24 KD mice that developed metastasis, MMP24 expression was detected in a subpopulation of cells at the primary site, suggesting that certain cells either escaped initial MMP24 silencing or re-activated MMP24 after initial KD (Supplementary Fig. 10g, 10p). We next studied an $EGFR^{L858}$ patient-derived xenograft (PDX), derived from a patient with metastatic LA[23]. IHC analysis of the PDX revealed robust MMP24 staining (Supplementary Fig. 11a). When orthotopically implanted, we observed overt primary tumor formation and spontaneous metastasis to the contralateral lung (Fig. 4l). Moreover, we found a functional role for MMP24 in promoting metastasis in our PDX, as *MMP24* KD decreased invasion of tumor cells derived from this $EGFR^{L858}$ PDX (Fig. 4m, Supplementary Fig. 11b–c). Our data suggest that the CIC-ETV4 downstream effector MMP24 promotes metastasis across multiple LA models.

Functional suppression of CIC de-represses ETV4-MMP24 to promote tumor progression

To determine if CIC expression correlates with LA progression, we performed CIC IHC analysis in a human lung TMA[24]. We found decreased nuclear CIC expression in LA specimens (stage I–III; n=130) compared with normal tissue (n=126), which correlated with increased MMP24 expression in these tumors (Figure 5a, Supplementary Fig. 12a–c). Using NSCLC mRNA datasets[19], we observed worse PFS specifically in unselected patient tumors with high levels of *ETV4* compared to those with low *ETV4* (Fig. 5b, Supplementary Fig. 12d). Additionally, we observed a positive correlation between ETV4 and MMP24 in the TCGA LA dataset (Supplementary Fig. 12e). Interestingly, we did not observe a correlation between decreased CIC mRNA and either ETV4 or MMP24 mRNA expression in these datasets, suggesting an alternative mode of CIC regulation beyond transcriptional control.

Given this finding, coupled with a low frequency of *CIC* genetic alterations in LA, we investigated whether CIC levels are post-translationally regulated. Indeed, CIC can be functionally suppressed via post-translational modification, whereby ERK phosphorylates nuclear CIC to promote nuclear export and degradation and thereby relieve repression of CIC target genes (Fig. 5c)[25–27]. As most LAs (~60–70%) harbor genetic alterations that hyperactivate ERK[28], we reasoned that ERK-mediated post-translational suppression of CIC may de-repress ETV4-MMP24 in cancers with genetically-intact CIC. Since growth factor stimulation can promote ERK-mediated CIC suppression[25–27], we monitored nuclear CIC expression with time-lapse microscopy in H1975 M1 cells expressing CIC-GFP during epidermal growth factor (EGF)-stimulated ERK activation. GFP-tagged CIC was expressed

in the nucleus at baseline, and this expression decreased upon EGF-stimulation (Fig. 5d). We did not observe cytoplasmic accumulation, but instead a rapid decrease in CIC protein expression upon ERK activation (Fig. 5e, Supplementary Fig. 13a). In concordance, we found that proteasome inhibition with bortezomib or MEK inhibition with trametinib could rescue EGF-mediated CIC degradation (Fig. 5f–g, Supplementary Fig.13b–c). Additionally, ERK signaling inhibition with rociletinib increased CIC and reduced *ETV4* promoter activity, leading to decreased ETV4 and MMP24 expression in H1975 cells (Fig. 5h–i). Reciprocally, EGF stimulation of serum starved H1975 cells resulted in decreased CIC expression (Supplementary Fig. 13d). Moreover, ERK inhibition with trametinib augmented CIC and decreased ETV4, MMP24, and invasion in *Kras* mutant A549 cells, without impacting growth (Supplementary Fig. 13e–g). These data suggest that ERK mediated CIC suppression de-represses the ETV4-MMP24 axis to enhance metastasis in LAs with hyperactive MAPK signaling, augmenting the role of CIC in NSCLC progression beyond those tumors with genetically altered CIC.

The CIC-ETV4-MMP24 metastatic axis is engaged in gastric adenocarcinoma

Analysis of TCGA tumors revealed a high frequency of *CIC* alterations in gastric adenocarcinoma (GA). We found that 26% (75/287) of GA cases harbored *CIC* genetic alterations (homozygous deletion (n=3) + nonsense/frameshift/missense mutation (26 tumors with 29 total mutations) + hemizygous loss (n=46) (Fig. 6a)[29]. Consistent with a functional role for CIC inactivation in promoting tumor progression, deleterious *CIC* alterations - truncations and homozygous deletions - were more frequently observed in advanced-stage GA (Fig. 6b). To correlate CIC expression with GA progression, we assessed nuclear CIC expression in 84 human GA specimens (stage I (n=15), stage II (n=54), stage III (n=15)) and 80 normal tissues. Decreased CIC expression correlated with GA progression (Fig. 6c, Supplementary Fig. 14a). To test whether CIC loss promotes aggressive metastatic gastric cancer progression, we studied publically-available mRNA datasets and found that specifically advanced-stage patients with low *CIC* expression had worse OS (Fig. 6d, Supplementary Fig. 14b–c)[30]. Thus, decreased CIC may promote lethal metastatic GA progression. We further investigated whether CIC loss was linked to increased ETV4 and MMP24 in gastric cancer. Indeed ETV4 and MMP24 expression was increased in tumors with CIC CN loss in the TCGA dataset (Fig. 6e–f)[29]. While we did not identify a correlation between *ETV4* or *MMP24* with survival in stage IV GA patients, high *ETV4* and *MMP24* expression were more broadly implicated as biomarkers of worse outcomes across all GA stages (Fig. 6g–h, Supplementary Fig. 14d–g). Additionally, we studied GA TMAs and found increased MMP24 expression in LN metastasis compared to primary tumors (Supplementary Fig. 14h–i). Collectively, the data suggest that the CIC-ETV4-MMP24 axis we uncovered in LA may also regulate GA progression.

As the function of CIC and whether it controls ETV4 and MMP24 in GA are unknown, we overexpressed CIC in AGS cells (harboring CIC^{F780S}) and found that this suppressed the ETV4-MMP24 axis (Supplementary Fig. 14j–k). CIC overexpression decreased invasion, and re-expression of MMP24 in CIC-overexpressing AGS cells restored invasiveness (Fig. 6i). CIC overexpression did not suppress GA growth (Supplementary Fig. 14l). Further, the pro-invasive function of MMP24 is conserved in GA, as MMP24 KD decreased invasion but

not tumor growth (Fig. 6j, Supplementary Fig. 14m–n). These data reveal a context-specific role for CIC in GA progression and metastasis, and suggest that genetic or post-translational suppression of CIC can de-repress the pro-metastatic ETV4-MMP24 axis across cancer subtypes.

Conserved dysregulation of CIC targets in lung and gastric adenocarcinomas

We hypothesized that there may be a shared set of CIC-responsive genes in LA and GA. We first identified 1,844 downregulated genes in H1975 M1 cells upon CIC rescue (adjusted p-value $<10e^{-10}$, Supplementary Fig. 14a). A promoter survey of these 1,844 genes identified 267 putative CIC targets, which contained the CIC binding motif (T(G/C)AATG(G/A)A) (Supplementary Fig. 15a, Supplementary table 4). We investigated whether GAs and LAs with CIC inactivation harbored increased levels of these putative CIC targets. We defined a set of CIC-responsive genes by stratifying TCGA GA tumors into two groups: CIC CN loss versus CIC CN neutral, identifying 163 DE genes (absolute log2 fold change >0.79, FDR <0.10) (Supplementary Fig. 15a). Since MAPK signaling-mediated suppression of CIC is a predominant mode of CIC inactivation in LA, we stratified TCGA LAs by *K-Ras* mutant versus *K-Ras* wild-type, yielding 79 DE genes (absolute log2 fold change >0.79, FDR <0.10) (Supplementary Fig. 15a). Comparative analysis of the DE genes from GA and LA tumors revealed *ETV4* as a conserved CIC-responsive gene (Supplementary Fig. 15a). Thus, *ETV4* is a CIC target across GA (CIC genetic loss) and LA (post-translational CIC suppression). We then analyzed >4700 tumors across 12 different tumor types and found increased *ETV4* expression correlated with worse survival in tumors with CIC CN loss (Supplementary Fig. 15b and 15c)[31]. The data suggest convergent inactivation of CIC and consequent activation of its effector, ETV4, across distinct cancer subtypes.

Discussion

We established an *in vivo* orthotopic model to study spontaneous NSCLC metastasis, and identified CIC as a suppressor of tumor progression and metastasis. Our study establishes the utility of the orthotopic system to molecularly dissect mediators of spontaneous metastasis *in vivo*. We show that lung and gastric cancers suppress CIC to gain tumor cell-autonomous, MMP24-dependent metastatic competence. Our data reveal CIC, ETV4, and MMP24 as biomarkers of clinical progression, and provide the rationale for therapeutic strategies to augment CIC or block ETV4-MMP24 to suppress metastasis.

Beyond genetic inactivation, ERK-mediated suppression of CIC may promote metastasis by augmenting the ETV4-MMP24 axis (Fig. 7). Hence, the widespread MAPK pathway hyperactivation present in LA may, in part, explain the high and rapid metastatic propensity of NSCLC. Pharmacologic inhibition of MAPK signaling may suppress metastasis by restoring CIC-mediated repression of effectors ETV4 and MMP24 in tumors with genetically-intact CIC. These anti-metastatic effects of MAPK pathway blockade may be distinct from, or in addition to, an impact on cell growth. Our findings provide motivation to further explore the interplay between MAPK signaling and CIC function across cancer subtypes. Overall, our study offers mechanistic insight into the molecular basis of metastasis

and reveals new strategies to identify, monitor, and therapeutically block metastatic progression.

Online Methods

Orthotopic lung xenografts in immunodeficient mice

Six to eight week old female SCID CB.17 mice were purchased from Taconic (Germantown, NY). Specific pathogen-free conditions and facilities were approved by the American Association for Accreditation of Laboratory Animal Care. Surgical procedures were reviewed and approved by the UCSF Institutional Animal Care and Use Committee (IACUC), protocol #AN107889-02B.

To prepare cell suspensions for thoracic injection adherent tumor cells were briefly trypsinized, quenched with 10% FBS RPMI media and resuspended in PBS. Cells were pelleted again and mixed with Matrigel matrix (BD Bioscience Cat.356237) on ice for a final concentration of 1.0×10^5 cells/μl. The Matrigel-cell suspension was transferred into a 1ml syringe and remained on ice until the time of implantation.

For orthotopic injection, mice were placed in the right lateral decubitus position and anesthetized with 2.5% inhaled isoflurane. A 1 cm surgical incision was made along the posterior medial line of the left thorax, fascia and adipose tissue layers were dissected and retracted to expose the lateral ribs, intercostal space, and the left lung parenchyma. Upon recognition of left lung respiratory variation, a 30-guage hypodermic needle was used to advance through the intercostal space ~3 mm into the lung tissue. For human cancer cell lines, care was taken to inject 10μl (1.0×10^6 cells) of cell suspension directly into the left lung. For PDX orthotopic xenotransplantation, a single cell suspension was first prepared following whole tumor explant from the flanks of immunodeficient mice. Whole tumors were washed in PBS, minced with a sterile scalpel, incubated at 37 degrees in trypsin for 15 minutes, and triturated with a 25-guage syringe until cells could easily pass through the needle bore. The PDX cell suspension was washed with PBS and resuspended in Matrigel then aspirated into at 30-guage syringe and 10 μls was injected into the left lung. The needle was rapidly withdrawn and mice were observed for pneumothorax. Visorb 4/0 polyglycolic acid sutures were used for primary wound closure of the fascia and skin layer. Mice were observed post-procedure for 1–2 hours and body weights and wound healing were monitoring weekly[1].

In-vivo bioluminescence imaging

Mice were imaged at the UCSF Preclinical Therapeutics Core starting on post-injection day 7 with a Xenogen IVIS 100 bioluminescent imaging system. Prior to imaging, mice were anesthetized with isoflurane and intraperitoneal injection (IP) of 200μl of D-Luciferin at a dose of 150mg/kg body weight was administered. Weekly monitoring of bioluminescence of the engrafted lung tumors was performed until week 5. Radiance was calculated automatically using Living Image Software following demarcation of the thoracic cavity (ROI) in the supine position. The radiance unit of photons/sec/cm2/sr is the number of

photons per second that leave a square centimeter of tissue and radiate into a solid angle of one steradian (sr).

CTC collection and analysis

Mice were anesthetized with isofluorane, the mediastinum was sterilized with ethanol and a vertical incision was made from the sternal notch to the xyphoid process. A 25-gauge needle was used to puncture the right heart ventricle and aspirate 300μl of whole blood into a 1 mL syringe primed with 0.5M EDTA pH 8.0 and directly injected into a K2 EDTA coated BD Vacutainer (BD 367841). 100μl of whole blood was added to 5ml of 1× RBC lysis buffer, pelleted and resuspended in 5ml of PBS with 0.5% FBS. Cells were again pelleted and resuspended in 500μl of PBS and GFP positivity was measured on a BD LSRII flow cytometer.

Ex-vivo bioluminescence imaging

Mice were injected IP with 200 μl (150mg/kg) of D-Luciferin and subsequently sacrificed at 5 weeks, en-bloc resection of the heart and lungs was performed following intracardiac puncture and whole blood collection. The heart was removed and the right and left lung lobes were separated with a midline incision through the trachea. Hind limbs were harvested and imaged in mice with detectable luminescence. Imaging was performed in a 12 well tissue culture plate with Xenogen IVIS 100 bioluminescent imaging.

Magnetic resonance imaging

All studies were performed in accordance with the guidelines of the UCSF IACUC protocol, #AN107889-02B. Mice were anesthetized with 2.5% inhaled isoflurane and maintained on 1.5% throughout data collection. Images were obtained every two weeks using the Agilent 7T 300 MHz Horizontal Bore Varian MR System at the UCSF Small Animal MRI facility.

Experimental Tail Vein Lung Colonization Assay

The animal protocol was approved by the UCSF IACUC, #AN107889-02B. The tail-vein of 6–8 week old female SCID mice was injected with 5×10^5 cells resuspended in 100μl of sterile PBS. Lung colonization was monitored weekly following IP injection of D-Luciferin by Xenogen IVIS 100 bioluminescent imaging system.

Cell lines and culture reagents

Cell lines were obtained, authenticated, and cultured as recommended by the American Type Culture Collection (ATCC). All cell lines were tested and negative for mycoplasma. H1975 (*EGFR*$^{L858R,\ T790M}$), A549 (*KRAS*^{G12S}), HCC364 (*BRAF*^{V600E}), H3122 (EML4-ALK variant 1), and AGS cells were obtained from ATCC. H1975 10-1 and H1975 1-1 metastatic derivatives were obtained from Clovis Oncology and renamed H1975 M1 and H1975 M2, respectively, both were engineered as previously described[2]. All cell lines were maintained at 37 °C in a humidified atmosphere at 5% CO_2 and grown RPMI 1640 media supplemented with 10% FBS, 100 IU/ml penicillin and 100ug/ml streptomycin.

Rociletinib was obtained from Clovis. EGF recombinant human protein was obtained from ThermoFisher.

Primary lung cancer sphere culture

Sphere cultures were derived from a previously established EGFR L858R PDX model[3] and cultured *in vitro* using our previously optimized tissue digestion and primary cell culture protocols[4]. Primary spheres were authenticated before the experiments validating the presence of the 2573 T>G -L858R mutation. For this analysis, the genomic DNA was extracted from the PDX spheres using Qiagen extraction kit (cat. number 51304); then the exon 21 was amplified by PCR and Sanger sequenced. Sequences for *EGFR* primers can be found in the Supplementary Primer table.

Gene knockdown and over-expression assays

All shRNAs were obtained from Sigma Aldrich. Sequences for individual shRNAs can be found in the Supplementary Primer table.

ON-TARGET plus ETV4 (L-004207-00-0005) and CIC (L-015185-01-0005) siRNAs were obtained from GE Dharmacon and transfection performed with Dharmafect transfection reagent per manufacture recommendations. *MMP24* cDNA was obtained from GE Dharmacon ORFeome (Clone ID 100069144) and subcloned into a pBABE puromycin retroviral vector using Gateway technology. The entire *MMP24* coding sequence was confirmed in forward and reverse directions. ETV4 cDNA was obtained from GE Dharmacon (MGC Clone ID 3854349). ETV4 sequence was confirmed in the forward and reverse directions. *CIC* cDNA was obtained from OriGene and subcloned into a lentiviral vector with a c-terminal monomeric GFP tag (OriGene RC215209L2). Lentiviral GFP-tagged ERF was obtained from GeneCopoeia (EX-S0501-Lv122).). Lentiviral GFP-tagged PAFAH1B3 was obtained from GeneCopoeia (EX-M0513-Lv122). The lentiviral GFP-Luciferase vector was a kind gift from Michael Jensen (Seattle Children's Research Institute, Seattle). The lentiviral luciferase vector was obtained from Addgene (#21471). Fugene 6 transfection reagent was used for all virus production and infection was carried out with polybrene.

Luciferase promoter assay

293T cells were obtained from ATCC. Cells were grown in Dulbecco's modified Eagle Medium (DMEM), supplemented with 10% FBS, 100 IU/ml penicillin and 100ug/ml streptomycin in a 5% CO_2 atmosphere. Cells were split into a 96 well plate to achieve 50% confluence the day of transfection. LightSwitch luciferase assay system (SwitchGear Genomics) was used per the manufactures protocol. Briefly, a mixture containing FuGENE 6 transfection reagent, 50ng Luciferase GoClone MMP24 promoter (1232 bp upstream of the start site) plasmid DNA, 50ng of either control (empty) vector or fully sequenced ETV4 cDNA (Dharmacon Clone ID 3854349) was added to each well. All transfections were performed in quintuplicate. For ETV4 luciferase promoter assay, the LightSwitch luciferase assay system was used per manufactures protocol. H1975, cells were transfected with 50ng luciferase GoClone ETV4 promoter 24 hours before treatment with rociletinib and assessed for luciferase activity after 6 hours of treatment.

Western blot and qRT-PCR

All immunoblots represent at least two independent experiments. Adherent cells were washed and lysed with RIPA buffer supplemented with proteinase and phosphatase inhibitors. Proteins were separated by SDS-PAGE, transferred to Nitrocellulose membranes, and blotted with antibodies recognizing: MMP24 (R&D – AB924), AXL (Cell Signaling – C89E7), GFP (Cell Signaling – D5.1), E-Cadherin (Cell Signaling – 24E10), Vimentin (Cell Signaling – D21H3), HSP90 (Cell Signaling – C45G5), ETV4 (Lifespan – LSB1527), Actin (Sigma – clone AC-74), N-Cadherin (Cell Signaling - 4061), Myc-tag (Cell Signaling – 71D10) and CIC (Acris - AP50924PU-N).

For EGF stimulated time-course H1975 M1 GFP-tagged CIC expressing cells were serum starved for 3 hours, followed by EGF (100ng/ml) stimulation for 0, 15, 30, 45, and 60 minutes. For H1975 parental cells, serum starvation was performed for 3 hours, followed by EGF (100ng/ml) stimulation for 30 minutes. For bortezomib and trametinib pre-treatment experiments, H1975 M1 GFP-tagged CIC expressing cells were pre-treated with bortezomib or trametinib for 6 hours, followed by addition of EGF (100ng/ml) for 0, 15, 30, 45, and 60 minutes. Lysates were collected in RIPA buffer as described above.

For drug treatments, H1975 were treated with either DMSO or rociletinib and lysates were collected in RIPA buffer and western blot performed as detailed above.

Image J was used to quantify all western blots.

Isolation and purification of RNA was performed using RNeasy Mini Kit (Qiagen). 500 ng of total RNA was used in a reverse transcriptase reaction with the SuperScript III first-strand synthesis system (Invitrogen). Quantitative PCR included four replicates per cDNA sample. Human *MMP24, CIC, AXL, CDH1, VIM, ETV1, ETV4, ETV5*, and endogenous controls *GAPDH* or *TBP*, were amplified with Taqman gene expression assay (Applied Biosystems). Expression data was acquired using an ABI Prism 7900HT Sequence Detection System (Applied Biosystems). Expression of each target was calculated using the $2^{-\Delta\Delta Ct}$ method and expressed as a relative mRNA expression.

Genomic DNA amplification

Genomic DNA was extracted from H1975, H1975 M1, and H1975 M2 cells using the Qiagen QIAmp DNA Mini Kit. 150ng of total genomic DNA was used per reaction. To isolate single cells from the bulk H1975 parental population we used flow cytometry based cell sorting (individual H1975 cells were directly sorted into a single well of a 96-well plate and clonally cultured to generate independent single-cell derived subclonal cultures). We next extracted genomic DNA from these individual H1975 subclones and performed targeted PCR amplification of exon 4 and the flanking introns of CIC. *CIC* and *GAPDH* primer sequences can be found in the Supplementary primer table.

Chromatin immuprecipitation and PCR (ChIP-PCR)

ChIP was performed on H1975 M1 and H1975 cells with the SimpleChIP Enzymatic Chromatin IP kit, Cell Signaling Technology #9003. The CIC antibody used for IP was obtained from Acris AP50924PU-N. The ETV4 antibody used for IP was obtained from

Aviva Systems Biology (ARP32263). Promoter primer sequences for ETV4, ETV5, and MMP24 can be found in the Supplementary Primer table.

CIC site directed mutagenesis

QuikChange II mutagenesis kit (Agilent) was used to generate all CIC mutants in a pCMV6 expression vector, Origene #RC215209. We used the QuikChange II primer design website to generate mutagenesis primers for the following mutants. For transient transfection experiments, Fugene 6 transfection reagent was used and stable expressing clones were derived with G418 selection for *in vivo* experiments. Primer sequences for individual mutants can be found in the Supplementary Primer table.

Transwell migration and invasion assays

RPMI with 10% FBS was added to the bottom well of a trans-well chamber. 2.5×10^4 cells resuspended in serum free media was then added to the top 8 μm pore matrigel coated (invasion) or non-coated (migration) trans-well insert (BD Biosciences). After 20 hours, non-invading cells on the apical side of inserts were scraped off and the trans-well membrane was fixed in methanol for 15 minutes and stained with Crystal Violet for 30 minutes. The basolateral surface of the membrane was visualized with a Zeiss Axioplan II immunofluorescent microscope at 10×. Each trans-well insert was imaged in five distinct regions at 10× and performed in triplicate. % invasion was calculated by dividing the mean # of cells invading through Matrigel membrane / mean # of cells migrating through control insert.

Immunostaining (IHC): orthotopic lung tissue, patient derived specimens, and tissue microarray (TMA)

Mice were sacrificed at the primary endpoint (5 weeks). Lungs were harvested en-bloc and dissected along the mediastinum to separate the right and left lung lobes. Immediately following ex-vivo imaging, lungs were fixed in 10% neutral buffered formalin for 72 hours, embedded in paraffin and 5–10 μm sections were prepared. Sections were subsequently de-paraffinized and incubated with antibodies directed against MMP24 (R&D – AB924), GFP (Cell Signaling – D5.1), CIC (Acris – AP50924PU-N), and EGFR L858R (Cell signaling – 43B2) overnight.

Formalin fixed, paraffin embedded (FFPE) patient derived tumor specimens were obtained under the auspices of institutional review board (IRB)-approved clinical protocols. Specimens were de-paraffinized and stained with an antibody against MMP24 (R&D).

Two lung cancer tissue microarrays with primary tumor and lymph node metastasis (LC817 and LC814) and two TMAs with lung tumors and adjacent normal tissue (HLug-Ade150Sur-01 and HLug-Ade150Sur-02) were obtained from Biomax and stained for MMP24 (R&D) and CIC (Acris) antibodies. Each sample stained with MMP24 was scored as negative (0), weak (1), moderate (2), strong (3), very strong (4) according to staining intensities. CIC (Acris) expression was assessed through IHC using nuclear H-Score (3 × percentage of strongly staining nuclei + 2 × percentage of moderately staining nuclei + percentage of weakly staining nuclei). To generate correlation plots between CIC and

MMP24 in the TMAs we compared the IHC scores of the paired samples using the 0–4 scoring system.

One gastric cancer TMA (ST810b) was stained with MMP24 antibody (R&D) and two gastric (ST1504 and ST1505) tissue microarrays with tumor, normal adjacent tissue, and clinical stage was obtained from Biomax was stained with CIC (Acris). Quantification of IHC intensity was scored in a similar fashion to the lung TMAs. All TMAs were scanned and viewed using Spectrum software.

Immunofluorescence

Immunofluorescence was performed on formalin fixed, paraffin embedded lung tissue with primary antibodies against GFP (rabbit mAb, Cell Signaling) and human specific Vimentin (mouse mAb, Santa Cruz (V9)) followed by fluorescently conjugated secondary antibodies (Invitrogen). ProLong Gold Antifade Mountant with DAPI was applied directly to fluorescently labeled tissue on microscope slides. Fluorescent images were collected on Zeiss Axioplan II fluorescent microscope.

Time-lapse microscopy

Time-lapse images were captured on a Nikon Ti-E Microscope, incubated at 37 degrees celsius and 5% CO2. Images were taken every 20 seconds for a 60 minute duration with or without EGF stimulation after 3 hours of serum starvation. Control images of H1975 M1 GFP expressing cells with EGF and H1975 M1 CIC.GFP expressing cells without EGF stimulation were monitored over 60 minutes.

Cell Viability

Cells were seeded overnight at a density of 3,000 cells per well in 96-well plates in RPMI 1640 media containing 10% FBS and treated with relevant agents for 72 hours. Cell viability was determined using the CellTiter-GLO assay according to the manufactures protocol. Each assay consisted of at least three replicate wells. For crystal violet assays, 100,000 cells were seeded per well in a 12-well plate (250,000 cells in a 6 well plate) and allowed to grow for five consecutive days. Cells were then fixed in 3.7% paraformaldehyde, followed by 0.05% Crystal Violet stain. Quantification was performed using Image J software.

Proliferation assay

Cells were seeded overnight at a density of 1,000 cells per well in 96-well plates in RPMI 1640 media containing 10% FBS luminescence assessed on day 1, 3, 5, and 7 by CellTiter-GLO assay according to the manufactures protocol. Luminescence on day 3, 5, and 7 were normalized to day 1 to obtain a relative value. Each assay consisted of at least three replicate wells.

Expression profiling

Gene expression quantification from paired-end RNAseq data was performed on parental H1975 cell lines, and compared to H1975 derivative lines M1 and M2, using RSEM[5]. RNAseq datasets were deposited into GEO (GSE74866). Similarly, the H1975 M1 transcriptome was also compared to H1975 M1 with CIC reconstitution to obtain CIC

responsive genes. Genes were ranked according to significance of differential expression between parental and derived lines using DESeq.

Functional annotation and clustering was performed using the Database for Annotation, Visualization, and Integrated Discovery (DAVID). The top 1000 differentially expressed genes between H1975 and M1 or M2 was used to derive two independent gene lists. Both lists were entered into DAVID to generate two independent functional clustering lists with associated enrichment *P*-values[6]. GeneTrail GO analysis was performed using the same 1000 differentially expressed genes between parental H1975 and H1975 M1 or M2. GeneTrail GO analysis was performed using the top 1500 differentially expressed genes between H1975 M1 and H1975 M1 with CIC reconstitution[7].

Copy number segmentation of parental and derived exomes from paired-end DNAseq data was performed using CNVkit[8] CN analysis was deposited in GEO (GSE74866).

The Cancer Genome Atlas Data Analysis

Mutational analysis was performed using the cBio Cancer Genomics Portal[9]. Lung (n = 521) and stomach (n=287) adenocarcinoma datasets were used to search for mutations and copy number variations (CNVs) in the CIC gene. Using the cBio lung and stomach adenocarcinoma datasets, CIC frameshift and nonsense mutations were identified and clinical stage was manually verified for each TCGA specimen. Mutation analysis of advanced, metastatic lung adenocarcinomas (n=1,342) were obtained from Foundation Medicine.

CIC, ETV4, and MMP24 correlative expression analysis

Data preparation. TCGA RNAseq RSEM (v2) gene expression measurements were downloaded from the Firehose portal on August 28th 2015. Stomach/gastric cancer samples were unavailable from firehose and were instead downloaded from the TCGA DCC portal. Transcripts per million (TPM) expression values used in the analysis were calculated by multiplying every gene's scaled estimate by 10^6. Dataset was quantile-normalized to minimize potential batch effects. Gistic2 discretized copy number calls were downloaded from the Firehose portal on May 27th 2014.

Expression analysis. Expression levels of MMP24 and ETV4 after normalization were compared between patient samples with either single or double copy number loss for CIC to patients with copy number neutral CIC. P-values were calculated using a Mann–Whitney–Wilcoxon rank sum test comparing the expression values in patient samples with copy-loss to the copy normal samples.

Analysis of Copy Number Alteration in H1975, H1975 M1, and H1975 M2

Copy number alterations were first generated from Control-FREE Copy Number Caller (Control-FREEC) using the normalized distribution of reads to determine differences in coverage of whole exome sequence between normal and H1975, H1975 M1 or H1975 M2[10]. We then employed the previously published Shiny application (https://malinost.shinyapps.io/CNPupload) to visualize Control-FREEC profiles[11]. The Shiny program uploaded the ratios

from the Control-FREEC file and allowed direct visualization through R based chromosome plots. Once H1975, H1975 M1 or H1975 M2 Control-FREEC files were uploaded into the Shiny application we then set the parameters to achieve visualization of chromosome 19 with a range set to optimally locate CIC (chromosome 19 position 42,772,689 – 42,799,949 in human GRCH37/hg19).

Establishment of CIC responsive gene set

Gene expression quantification from paired-end RNAseq data was performed on H1975 M1 CIC null cells and compared to H1975 M1 with CIC reconstitution using RSEM[12]. Genes were ranked according to significance of differential expression using DESeq. 1,844 significantly downregulated genes (adjusted p-value $<10e^{-10}$) were identified and subsequently surveyed for the CIC binding consensus sequence (T(G/C)AATG(G/A)A) in the promoter region (−2000 ~100 relative to TSS,), sequences were download from eukaryotic promoter database (http://epd.vital-it.ch/).

CIC mutation analysis in early and advanced stage lung adenocarcinoma

For CIC mutation identification in the TCGA, the lung adenocarcinoma provisional dataset was used to identify early stage (I–II) and advanced stage (III–IV) tumors. A total of five patients TCGA-69-7980-01, TCGA-97-7547-01, TCGA-64-5779-01, TCGA-75-6214-01, and TCGA-86-8056-01 were identified in 488 patients with clinical stage and CIC mutational analysis available.

For the Rizvi cohort, we used cBio portal to identify tumors with mutations in CIC, JB112852 and ZA6965.

Differential expression of lung and gastric adenocarcinoma TCGA datasets

The normalized gene expression TCGA datasets for lung adenocarcinoma (LUAD_exp_HiSeqV2_PANCAN-2015-02-24), stomach adenocarcinoma (TCGA_STAD_exp_HiSeq-2015-02-24) along with stomach somatic copy number data (TCGA_STAD_gistic2_thresholded-2015-02-24) were downloaded from UCSC cancer genome browser. For lung cancer, the samples were stratified into KRAS mutation and KRAS wildtype subgroups, for stomach cancer, samples were stratified into CIC_loss and CIC normal subgroups, samples with CIC gain were excluded from analysis. Limma R package was used for differential gene expression analysis, significantly differentially expressed genes between these two subgroups were generated with absolute log2 fold change greater than 0.79 and FDR (Benjamini-Hochberg adjustment) less than 0.1 cut-off.

Differential expression and survival analysis of the pan-cancer TCGA dataset

Pan-cancer TCGA dataset (TCGA_PANCAN12_copynumber-2015-01-28) was downloaded from UCSC cancer genome browser. Pan-cancer samples were stratified into CIC_loss and CIC_normal subgroups, samples with CIC gain were excluded from analysis. Samples in each subgroup were then stratified based on ETV4 expression level.

To correlate ETV4 expression with overall survival in the pan-cancer dataset. We computed the median ETV4 expression level across all samples. Samples above the median were

defined as ETV4 High, below the median as ETV4 Low. Log-rank test was used to establish a p-value in Kaplan-Meier overall survival curve.

Lung and Gastric cancer survival analysis

Kaplan-Meier curves for lung and gastric cancer overall survival (OS) and time to first progression (PFS) were generated using the Kaplan-Meier Plotter database[13,14] The "recommended" MMP24 probe (213171_s_at) was used in all KM plots. To identify lymph node positive NSCLC patients in our study, we selected AJCC stage N1 patients for analysis. We used the 2015 version gene symbol: MMP24 probe 213171_s_at, survival: FP (n=982), auto select best cutoff, selected all histology, AJCC stage N1 (n=130). HAPLN1 probe 205523_at, WNT5A probe 213425_at, *COL8A1* probe 214587_at, and SLC1A3 probe 202800_at were used to generated NSCLC KM plots with AJCC stage N1 patients as performed for MMP24. No *ADAMTS10* probe was available for survival analysis. For "all comers" analysis in NSCLC (n=982) we used the following parameters: gene symbol: MMP24 probe 213171_s_at, survival: FP, auto select best cutoff, selected all histology, AJCC stage all (N = 982). For ETV4 in NSCLC we used the following selection criteria: KM plotter 2015 version, gene symbol: ETV4 probe 211603_s_at, survival: FP, auto select best cutoff, selected all histology, (N = 982) and gene symbol: ETV4 probe 211603_s_at, survival: FP, auto select best cutoff, selected all histology, AJCC stage N1 (N = 130).

For gastric cancer analyses and generation of PFS and OS KM survival curves we used the "recommended" MMP24 probe 213171_at_s, ETV4 probe 211603_s_at, and CIC probe 212784_s_at. For MMP24, ETV4, and CIC analyses in gastric cancer, all parameters were left at default settings with best cutoff auto selection for analysis. Stage IV patients with poorly differentiated gastric cancer were selected in an independent analyses of CIC, ETV4, and MMP24, all other settings were left as default with best cutoff auto selection.

Statistical analysis

Experimental data are presented as mean +/− SEM. P-values derived for all in-vitro experiments were calculated with either two-tailed Student's t test or one-way ANOVA test. Kaplan-Meier metastasis-free survival curves were calculated using Log-rank test.

For each *in vivo* experiment, including orthotopic studies, 10–15 mice were injected with each specified cell line as indicated and all were included in the final analysis. Non-engrafted mice, defined as no detectable luciferase activity two weeks post-implantation were excluded from final analysis. Pre-established criteria (time to metastasis) was used in all orthotopic cohorts. Mice were not randomized prior to intervention. Investigators were not blinded to the group allocation during the experiment or when assessing the outcome.

Supplementary Material

Refer to Web version on PubMed Central for supplementary material.

Acknowledgments

R.A.O. was supported by A.P. Giannini Foundation and NIHT32CA177555-01. T.G.B acknowledges support from the NIH Director's New Innovator Award DP2 CA174497, NIH/NCI RO1 CA169338, and Pew-Stewart Foundation Trusts. We thank B. Hann (UCSF Preclinical Therapeutics Core) for helpful discussions.

Potential conflicts of interest

HJH and ADS are employees of Clovis Oncology. KG, JS, VAM and SA are employees of Foundation Medicine. TGB is a consultant to Novartis, Astellas, Array Biopharma, Ariad, Teva, Astrazeneca, and has received research funding from Ignyta.

References

1. Herbst RS, Heymach JV, Lippman SM. Lung Cancer. N Engl J Med. 2008; 359:1367–1380. [PubMed: 18815398]
2. Chaffer CL, Weinberg RA. A perspective on cancer cell metastasis. Science. 2011; 331:1559–1564. [PubMed: 21436443]
3. Khanna C, Hunter K. Modeling metastasis in vivo. Carcinogenesis. 2005; 26:513–523. [PubMed: 15358632]
4. Francia G, Cruz-Munoz W, Man S, Xu P, Kerbel RS. Mouse models of advanced spontaneous metastasis for experimental therapeutics. Nat Rev Cancer. 2011; 11:135–141. [PubMed: 21258397]
5. Sequist LV, et al. Genotypic and Histological Evolution of Lung Cancers Acquiring Resistance to EGFR Inhibitors. Science Translational Medicine. 2011; 3:75ra26–75ra26.
6. Walter AO, et al. Discovery of a Mutant-Selective Covalent Inhibitor of EGFR that Overcomes T790M-Mediated Resistance in NSCLC. Cancer Discovery. 2013; 3:1404–1415. [PubMed: 24065731]
7. Zhang Z, et al. Activation of the AXL kinase causes resistance to EGFR-targeted therapy in lung cancer. Nature Genetics. 2012; 44:852–860. [PubMed: 22751098]
8. Madero-Visbal RA, et al. Bioluminescence imaging correlates with tumor progression in an orthotopic mouse model of lung cancer. Surg Oncol. 2012; 21:23–29. [PubMed: 20801643]
9. Mordant P, et al. Bioluminescent orthotopic mouse models of human localized non-small cell lung cancer: feasibility and identification of circulating tumour cells. PLoS ONE. 2011; 6:e26073. [PubMed: 22022511]
10. Gleize V, et al. CIC inactivating mutations identify aggressive subset of 1p19q codeleted gliomas. Ann Neurol. 2015; 78:355–374. [PubMed: 26017892]
11. Choi N, et al. miR-93/miR-106b/miR-375-CIC-CRABP1: a novel regulatory axis in prostate cancer progression. Oncotarget. 2015; 6:23533–23547. [PubMed: 26124181]
12. Jin Y, et al. EGFR/Ras Signaling Controls Drosophila Intestinal Stem Cell Proliferation via Capicua-Regulated Genes. PLoS Genet. 2015; 11:e1005634. [PubMed: 26683696]
13. Bettegowda C, et al. Mutations in CIC and FUBP1 contribute to human oligodendroglioma. Science. 2011; 333:1453–1455. [PubMed: 21817013]
14. Rizvi NA, et al. Cancer immunology. Mutational landscape determines sensitivity to PD-1 blockade in non-small cell lung cancer. Science. 2015; 348:124–128. [PubMed: 25765070]
15. Lee Y, et al. ATXN1 protein family and CIC regulate extracellular matrix remodeling and lung alveolarization. Dev Cell. 2011; 21:746–757. [PubMed: 22014525]
16. Greenlee KJ, Werb Z, Kheradmand F. Matrix metalloproteinases in lung: multiple, multifarious, and multifaceted. Physiol Rev. 2007; 87:69–98. [PubMed: 17237343]
17. Jimenez G, Shvartsman SY, Paroush Z. The Capicua repressor--a general sensor of RTK signaling in development and disease. J Cell Sci. 2012; 125:1383–1391. [PubMed: 22526417]
18. Egeblad M, Werb Z. New functions for the matrix metalloproteinases in cancer progression. Nat Rev Cancer. 2002; 2:161–174. [PubMed: 11990853]
19. Gyorffy B, Surowiak P, Budczies J, Lanczky A. Online survival analysis software to assess the prognostic value of biomarkers using transcriptomic data in non-small-cell lung cancer. PLoS ONE. 2013; 8:e82241. [PubMed: 24367507]

20. Hayashita-Kinoh H, et al. Membrane-type 5 matrix metalloproteinase is expressed in differentiated neurons and regulates axonal growth. Cell Growth Differ. 2001; 12:573–580. [PubMed: 11714638]
21. Elkin M, Vlodavsky I. Tail vein assay of cancer metastasis. Curr Protoc Cell Biol. 2001; Chapter 19(Unit 19.2)
22. Porlan E, et al. MT5-MMP regulates adult neural stem cell functional quiescence through the cleavage of N-cadherin. Nat Cell Biol. 2014; 16:629–638. [PubMed: 24952463]
23. Blakely CM, et al. NF-kappaB-activating complex engaged in response to EGFR oncogene inhibition drives tumor cell survival and residual disease in lung cancer. Cell Rep. 2015; 11:98–110. [PubMed: 25843712]
24. Schoppmann SF, et al. Downregulation of CIC does not associate with overexpression of ETV1 or MAP kinase pathway activation in gastrointestinal stromal tumors. Cancer Invest. 2014; 32:363–367. [PubMed: 24897389]
25. Astigarraga S, et al. A MAPK docking site is critical for downregulation of Capicua by Torso and EGFR RTK signaling. The EMBO Journal. 2007; 26:668–677. [PubMed: 17255944]
26. Futran AS, Kyin S, Shvartsman SY, Link AJ. Mapping the binding interface of ERK and transcriptional repressor Capicua using photocrosslinking. Proc Natl Acad Sci U S A. 2015; 112:8590–8595. [PubMed: 26124095]
27. Grimm O, et al. Torso RTK controls Capicua degradation by changing its subcellular localization. Development. 2012; 139:3962–3968. [PubMed: 23048183]
28. Network, T. C. G. A. R. Comprehensive molecular profiling of lung adenocarcinoma. Nature. 2015; 511:543–550.
29. Network, T. C. G. A. R. Comprehensive molecular characterization of gastric adenocarcinoma. Nature. 2014; 513:202–209. [PubMed: 25079317]
30. Szasz AM, et al. Cross-validation of survival associated biomarkers in gastric cancer using transcriptomic data of 1,065 patients. Oncotarget. 2016
31. Network, T. C. G. A. R. The Cancer Genome Atlas Pan-Cancer analysis project. Nat Genet. 2013; 45:1113–1120. [PubMed: 24071849]

References for Online Methods

1. Mordant P, et al. Bioluminescent orthotopic mouse models of human localized non-small cell lung cancer: feasibility and identification of circulating tumour cells. PLoS ONE. 2011; 6:e26073. [PubMed: 22022511]
2. Walter AO, et al. Discovery of a Mutant-Selective Covalent Inhibitor of EGFR that Overcomes T790M-Mediated Resistance in NSCLC. Cancer Discovery. 2013; 3:1404–1415. [PubMed: 24065731]
3. Blakely CM, et al. NF-kappaB-activating complex engaged in response to EGFR oncogene inhibition drives tumor cell survival and residual disease in lung cancer. Cell Rep. 2015; 11:98–110. [PubMed: 25843712]
4. Wei W, et al. Single-Cell Phosphoproteomics Resolves Adaptive Signaling Dynamics and Informs Targeted Combination Therapy in Glioblastoma. Cancer Cell. 2016; 29:563–573. [PubMed: 27070703]
5. Li B, Dewey CN. RSEM: accurate transcript quantification from RNA-Seq data with or without a reference genome. BMC Bioinformatics. 2011; 12:323. [PubMed: 21816040]
6. Huang DW, Sherman BT, Lempicki RA. Systematic and integrative analysis of large gene lists using DAVID bioinformatics resources. Nat Protoc. 2009; 4:44–57. [PubMed: 19131956]
7. Backes C, et al. GeneTrail--advanced gene set enrichment analysis. Nucleic Acids Res. 2007; 35:W186–W192. [PubMed: 17526521]
8. Talevich E, Shain AH, Botton T, Bastian BC. CNVkit: Copy number detection and visualization for targeted sequencing using off-target reads. 2014 bioRxiv.
9. Cerami E, et al. The cBio cancer genomics portal: an open platform for exploring multidimensional cancer genomics data. Cancer Discovery. 2012; 2:401–404. [PubMed: 22588877]

10. Boeva V, et al. Control-FREEC: a tool for assessing copy number and allelic content using next-generation sequencing data. Bioinformatics. 2012; 28:423–425. [PubMed: 22155870]
11. Fransson S, et al. Estimation of copy number aberrations: Comparison of exome sequencing data with SNP microarrays identifies homozygous deletions of 19q13.2 and CIC in neuroblastoma. Int J Oncol. 2016; 48:1103–1116. [PubMed: 26794043]
12. Li B, Dewey CN. RSEM: accurate transcript quantification from RNA-Seq data with or without a reference genome. BMC Bioinformatics. 2011; 12:323. [PubMed: 21816040]
13. Gyorffy B, Surowiak P, Budczies J, Lanczky A. Online survival analysis software to assess the prognostic value of biomarkers using transcriptomic data in non-small-cell lung cancer. PLoS ONE. 2013; 8:e82241. [PubMed: 24367507]
14. Szasz AM, et al. Cross-validation of survival associated biomarkers in gastric cancer using transcriptomic data of 1,065 patients. Oncotarget. 2016

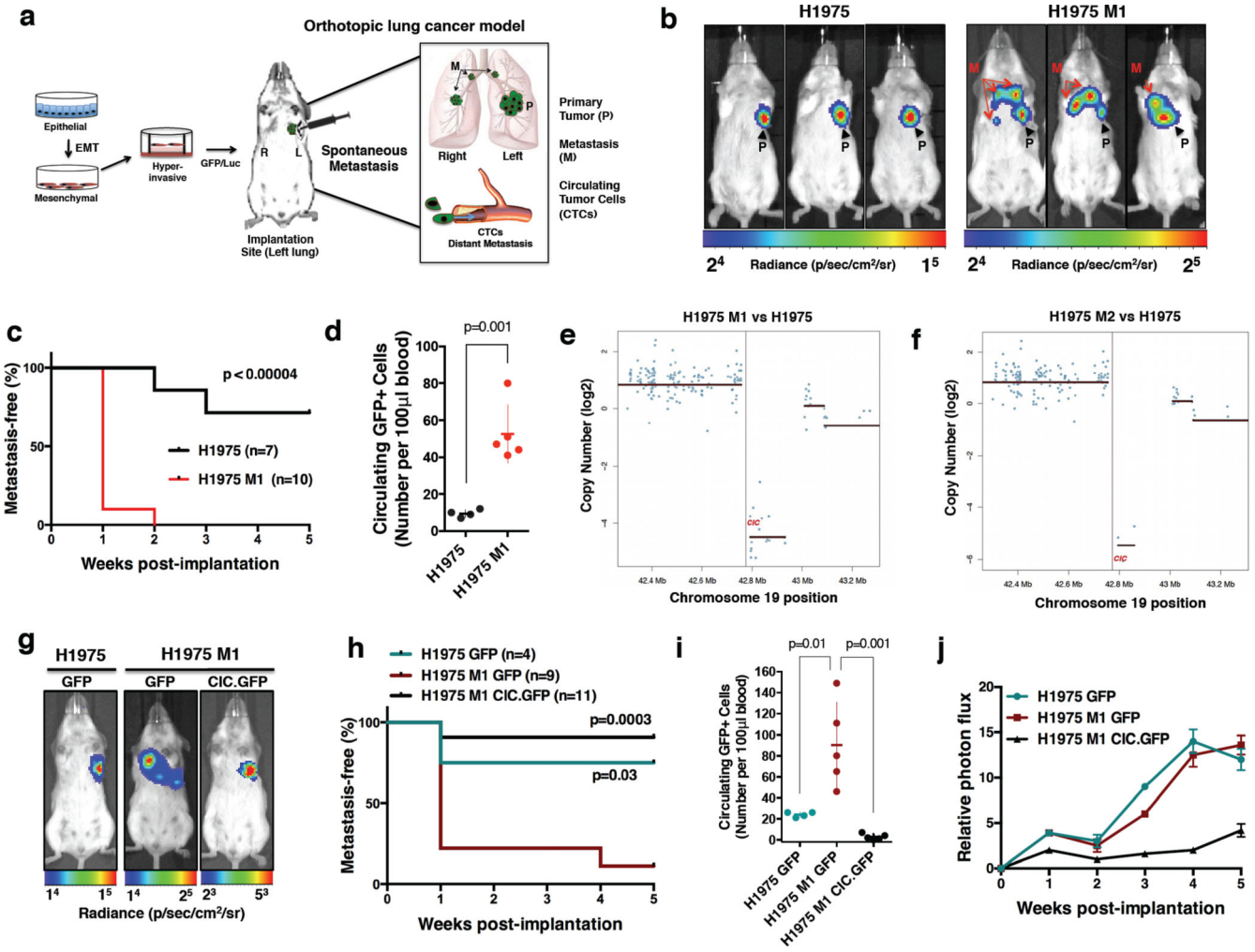

Figure 1. *In vivo* orthotopic model identifies novel effectors of lung cancer metastasis

(a) Orthotopic *in vivo* metastasis platform. (b) Bioluminescent images (BLI) of mice bearing H1975 GFP-Luc or H1975 M1 GFP-Luc cells. Left lung = implantation site; P = primary tumor; M = metastasis. (c) Metastasis-free survival comparing H1975 (n=7) and H1975 M1 (n=10) mice. p-value, log-rank. (d) Number of circulating GFP+ cells per 100 µl at 5 weeks post-implantation. Mean +/− SEM, 10 +/− 2 (H1975) and 52 +/− 7 (H1975 M1). p-values, Student's t-test. (e-f) Whole exome copy number profile at the CIC locus in H1975 M1 (e) and M2 (f) cells, compared to H1975 parental cells. (g) BLI of mice bearing H1975 GFP-Luc and H1975 M1 GFP-Luc expressing cells with either GFP control or GFP-CIC. Left lung = implantation site. (h) Metastasis-free KM curve comparing H1975 mice (n = 4) to H1975 M1 mice expressing GFP control (n = 9) or GFP-CIC (n = 11). p values, log-rank test. (i) Number of circulating GFP+ cells per 100 µl of blood at 5 weeks post-implantation. Mean +/− SEM, 24 +/− 1.2 (H1975 GFP), 90 +/− 18 (H1975 M1 GFP), and 3 +/− 1.2 (H1975 M1 CIC.GFP). p values, one-way ANOVA. (j) Normalized mean photon flux of H1975 GFP-luc or H1975 M1 mice expressing either GFP control or CIC.GFP over 5 weeks (from mice in g, h). Error bars reflect SEM.

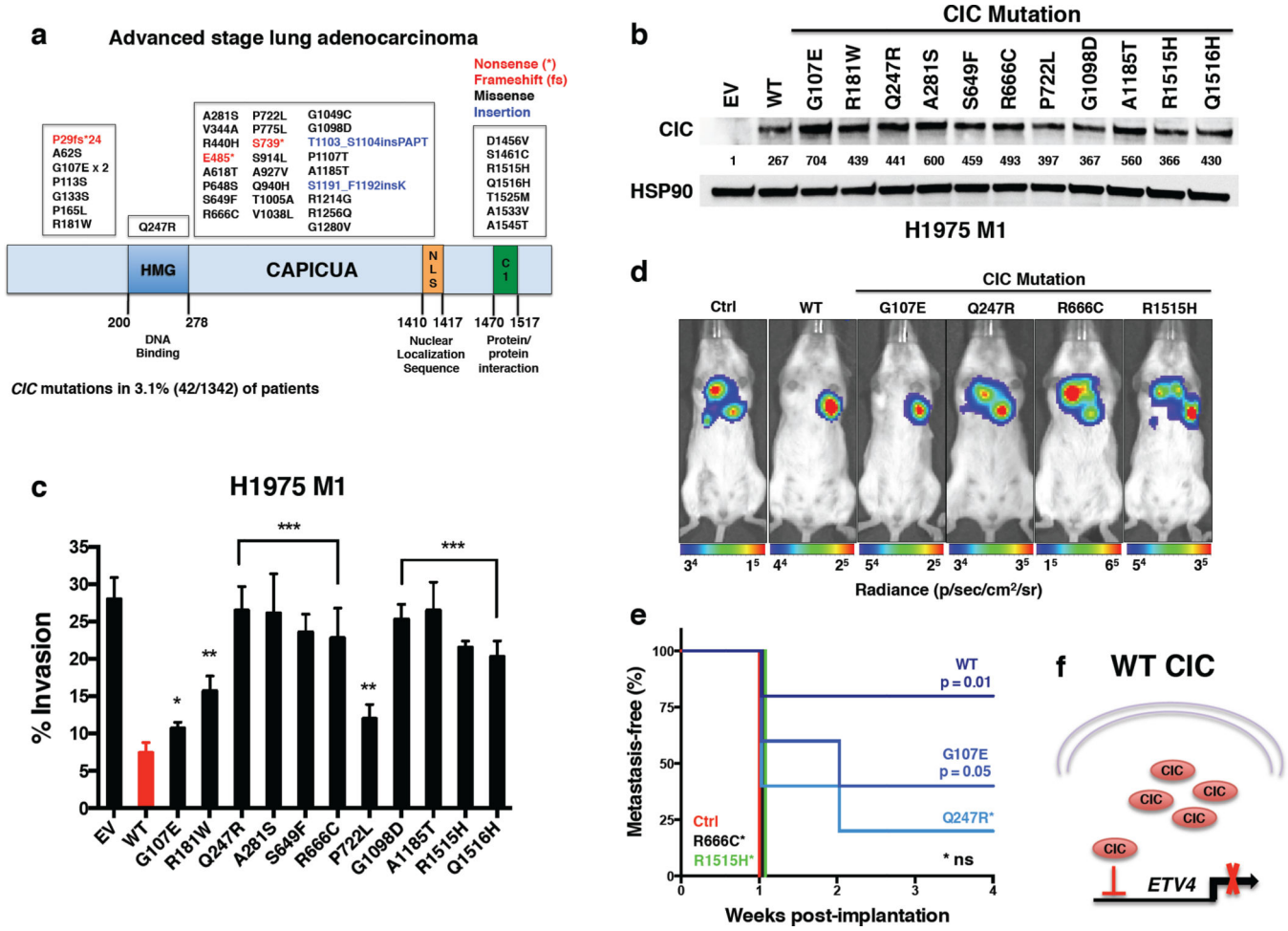

Figure 2. CIC is altered in advanced-stage lung adenocarcinoma

(a) CIC somatic mutations identified in advanced-stage human lung adenocarcinoma patient specimens. (b) Immunoblot of 11 myc-tagged CIC mutants compared to WT CIC and EV control in H1975 M1 cells. CIC quantification relative to EV control. (c) Invasion of H1975 M1 cells individually expressing the 11 CIC mutants compared to WT CIC and EV control. ***p=0.0001, **p=0.005, *p=0.03, p-values were calculated by one-way ANOVA compared to WT CIC. Error bars represent SEM. Results of two independent experiments in triplicate are shown. (d) BLI of mice orthotopically implanted with H1975 M1 cells expressing either Luciferase control (n=5), WT CIC (n=5), or CIC mutants G107E (n=5), Q247R (n=5), R666C (n=5), R1515H (n=5). (e) Metastasis-free survival comparing orthotopically implanted mice from (d). p-values, log-rank. (f) Depiction of CIC transcriptionally repressing ETV4 expression.

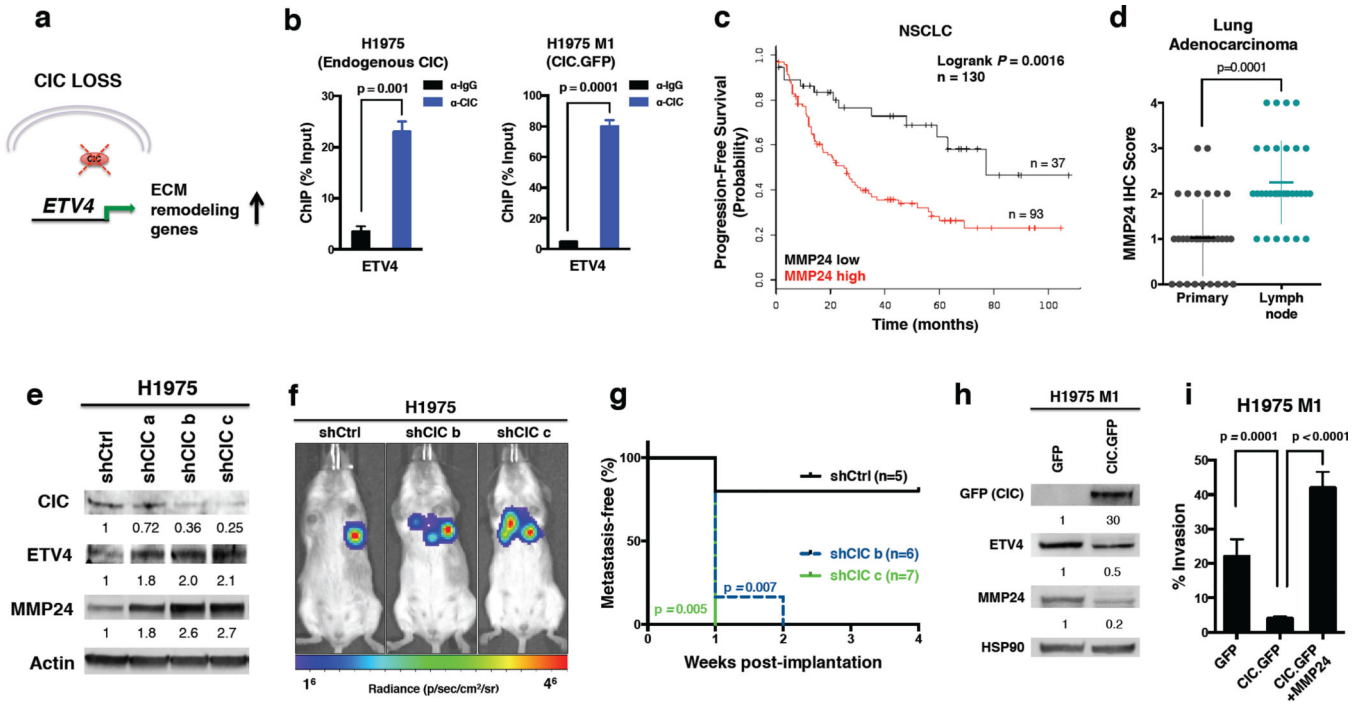

Figure 3. Inactivation of CIC de-represses an ETV4-MMP24 pro-metastatic circuit

(a) Inactivation of CIC de-represses ETV4 mediated transcription of ECM remodeling genes. (b) ChIP-PCR in H1975 and H1975 M1 cells demonstrating *ETV4* promoter occupancy by CIC in lung cancer cells. p-values, Student's t-test; error bars represent SEM. Data shown are representative of two independent experiments. (c) Progression-free survival for patients with LN positive (N1) NSCLC with high or low *MMP24* mRNA expression. n=130; p=0.0016. Probe 213171_s_at. (d) MMP24 IHC score of matched primary lung tumors and LN metastases from two independent TMAs. n=32 pairs (32 primary tumors, 32 LN metastasis). Mean 1.03 +/− 0.14 (primary) and 2.25 +/− 0.16 (LN metastasis). p value calculated by Student's t-test. (e) Immunoblots of H1975 parental cells expressing either shCtrl or shCICa, shCICb, or shCICc. (f) BLI of mice orthotopically implanted with H1975 cells expressing either Luciferase control (n=5), shCIC b (n=6), or shCIC c (n=7). (g) Metastasis-free surival of orthotopically implanted mice from (f). p values, log-rank. (h) Immunoblots of H1975 M1 cells expressing either GFP control or GFP-CIC. (i) Invasion of H1975 M1 cells expressing GFP control, GFP-CIC, or GFP-CIC with restored MMP24 expression (+MMP24). p-values, one-way ANOVA. Error bars represent SEM.

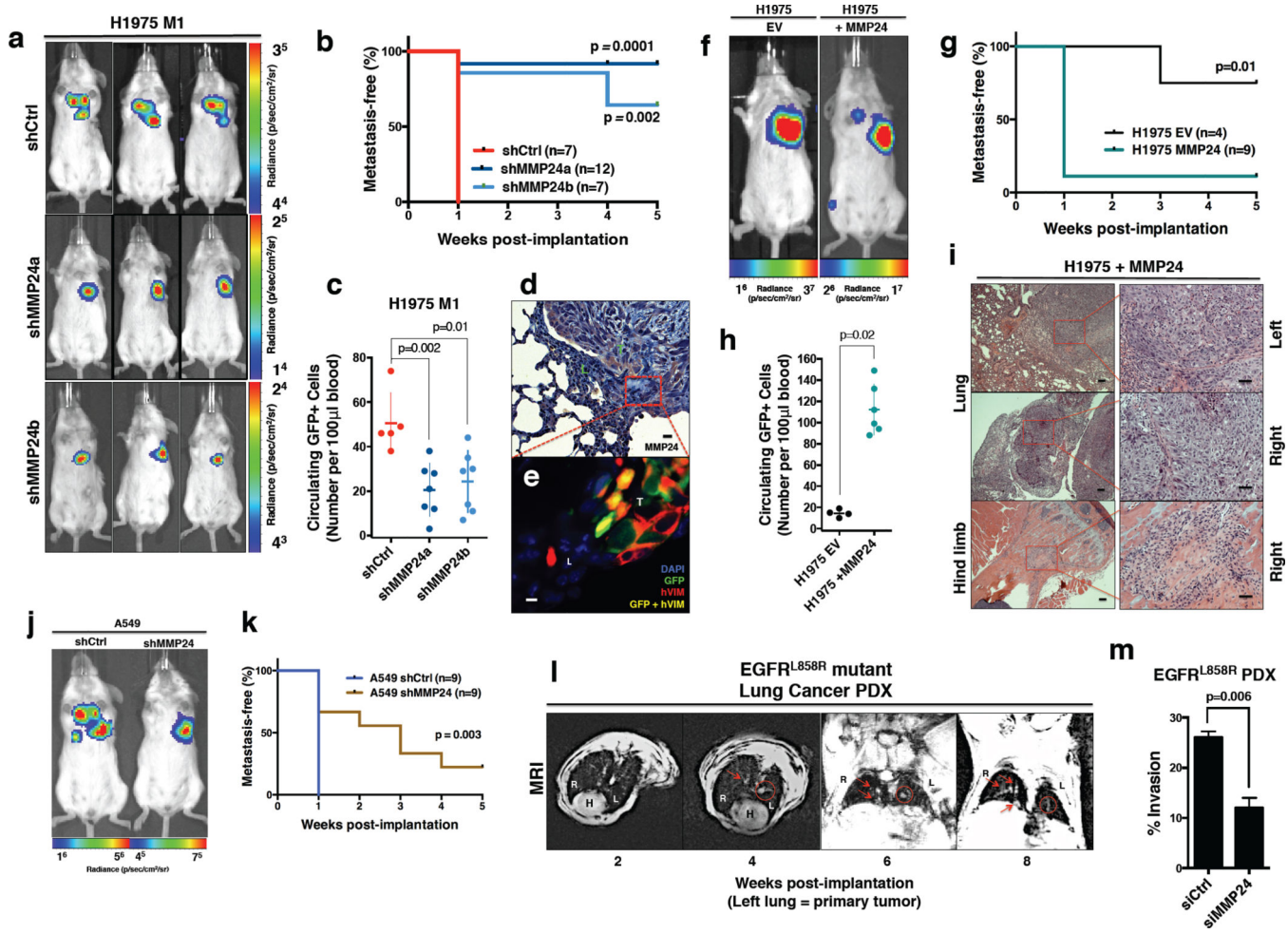

Figure 4. CIC effector MMP24 drives lung cancer metastasis

(a) BLI of shCtrl, shMMP24a, or shMMP24b expressing H1975 M1 mice. (b) Metastasis-free survival of H1975 M1 shCtrl (n=7), shMMP24a (n=12), or shMMP24b (n=7) mice. p-values, log-rank. (c) Circulating GFP+ cells/100 µl of blood at 5 weeks post-implantation. Mean +/− SEM, 51 +/− 6.1 (shCtrl, n=5), 20 +/− 4.5 (shMMP24a, n=7), 24 +/− 5.2 (shMMP24b, n=7). p-values, one-way ANOVA. (d) MMP24 staining of an orthotopically implanted tumor and mouse lung. T = tumor, L = lung. Scale bar, 50 µm (e) Tumor markers at the invasive edge. T = tumor, L = lung. Scale bar, 20 µm. (f) BLI of EV or MMP24 overexpressing H1975 GFP-Luc mice. (g) Metastasis-free survival of EV or MMP24-overexpressing H1975 mice. p-value, log rank. (h) Circulating GFP+ cells/100 µl of blood at 5 weeks post-implantation. Mean +/− SEM, 15 +/− 1.8 (EV, n=4) and 112 +/− 9.7 (+MMP24, n=6). p-value, Student's t-test. (i) H&E of H1975 +MMP24: primary tumor (left lung), metastasis (right lung and hind limb). Scale bars, 100 µm (left) and 50 µm (right). (j) BLI of shCtrl or shMMP24a A549 GFP-Luc mice. (k) Metastasis-free survival of shCtrl (n=9) or shMMP24a (n=9) expressing A549 mice. p values, log-rank. (l) MRI of mice orthotopically implanted with a LA PDX. Circle = primary, arrows = metastasis. H (heart), R (right lung), L (left lung). (m) Invasion of $EGFR^{L858R}$ PDX +/− MMP24 knockdown. p-values, student's t-test. Error bars represent SEM.

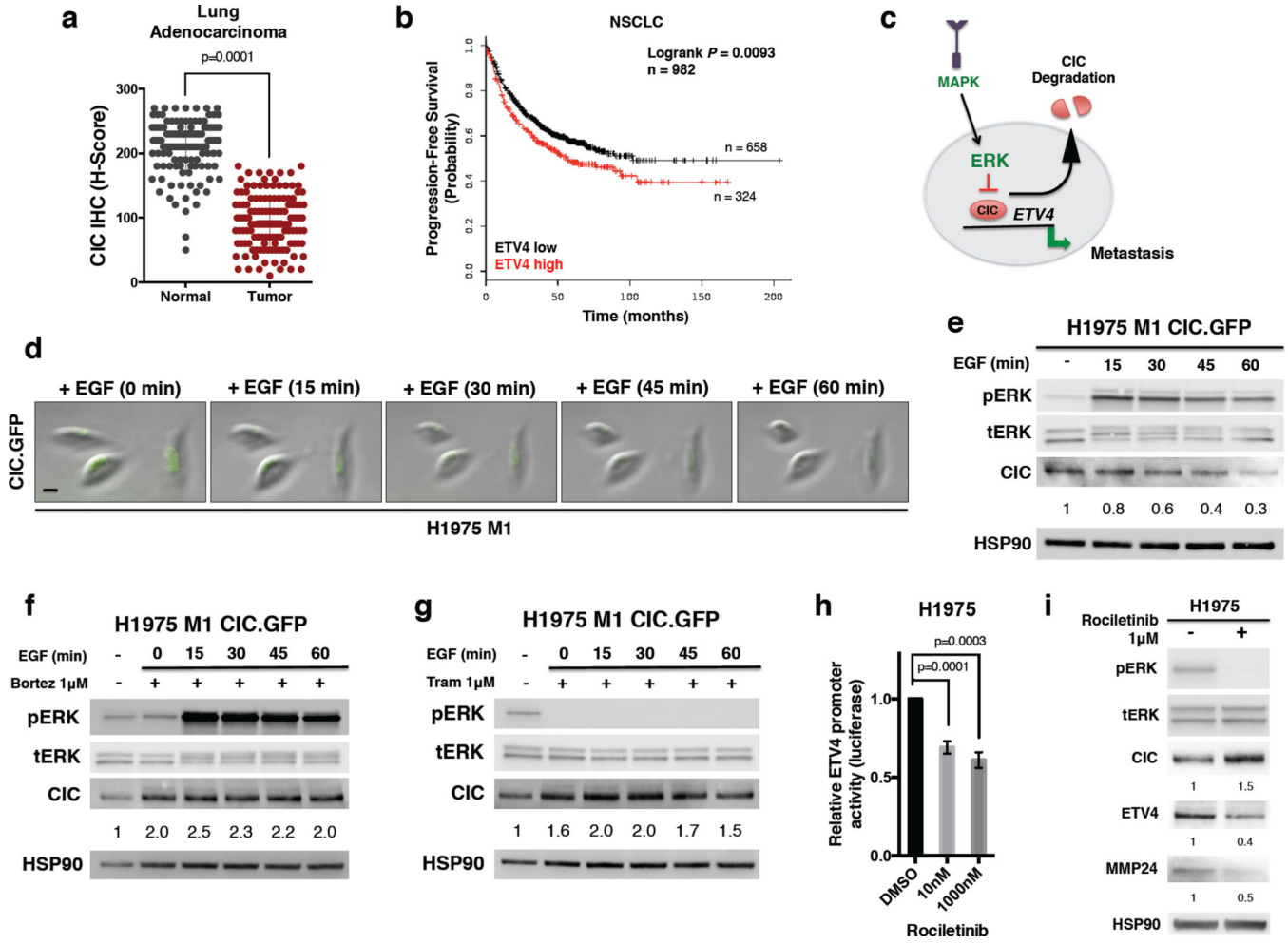

Figure 5. MAPK pathway activation functionally suppresses CIC

(a) Nuclear CIC expression (H-score) in 130 LA cases and 126 normal adjacent lung tissue specimens. Mean +/− SEM, 207 +/− 4.0 (normal) and 94 +/− 3.5 (tumor). p-values, Student's t-test. (b) PFS KM curve for lung cancer patients with either *ETV4* high or *ETV4* low mRNA expression. n = 982, p = 0.0093. Probe 211603_s_at. (c) Model of MAPK-ERK mediated functional suppression of CIC. (d) Time-lapse microscopy images of serum starved, EGF stimulated H1975 M1 cells expressing GFP-tagged CIC over the indicated intervals. Experiments were performed in duplicate with all CIC.GFP expressing cells (15/15) showing decreased nuclear GFP expression following EGF stimulation. Scale bar, 20 μm. Data show representative cells from two independent experiments. (e) Immunoblot time-course of EGF stimulated H1975 M1 cells expressing GFP-tagged CIC. Representative of two independent experiments. (f) Immunoblot time-course of EGF-stimulated H1975 M1 cells expressing GFP-tagged CIC, pretreated with bortezomib for 6 hours. Representative of two independent experiments. (g) Immunoblot time-course of EGF-stimulated H1975 M1 cells expressing GFP-tagged CIC, pretreated with trametinib for 6 hours. Representative of two independent experiments. (h) Relative ETV4 luciferase promoter activity in H1975 cells with DMSO or rociletinib treatment. p-values, one-way ANOVA. Error bars represent SEM,

n=5. (i) Immunoblots of H1975 cells treated with DMSO (−) or rociletinib (+) for 16 hours. Representative of two independent experiments.

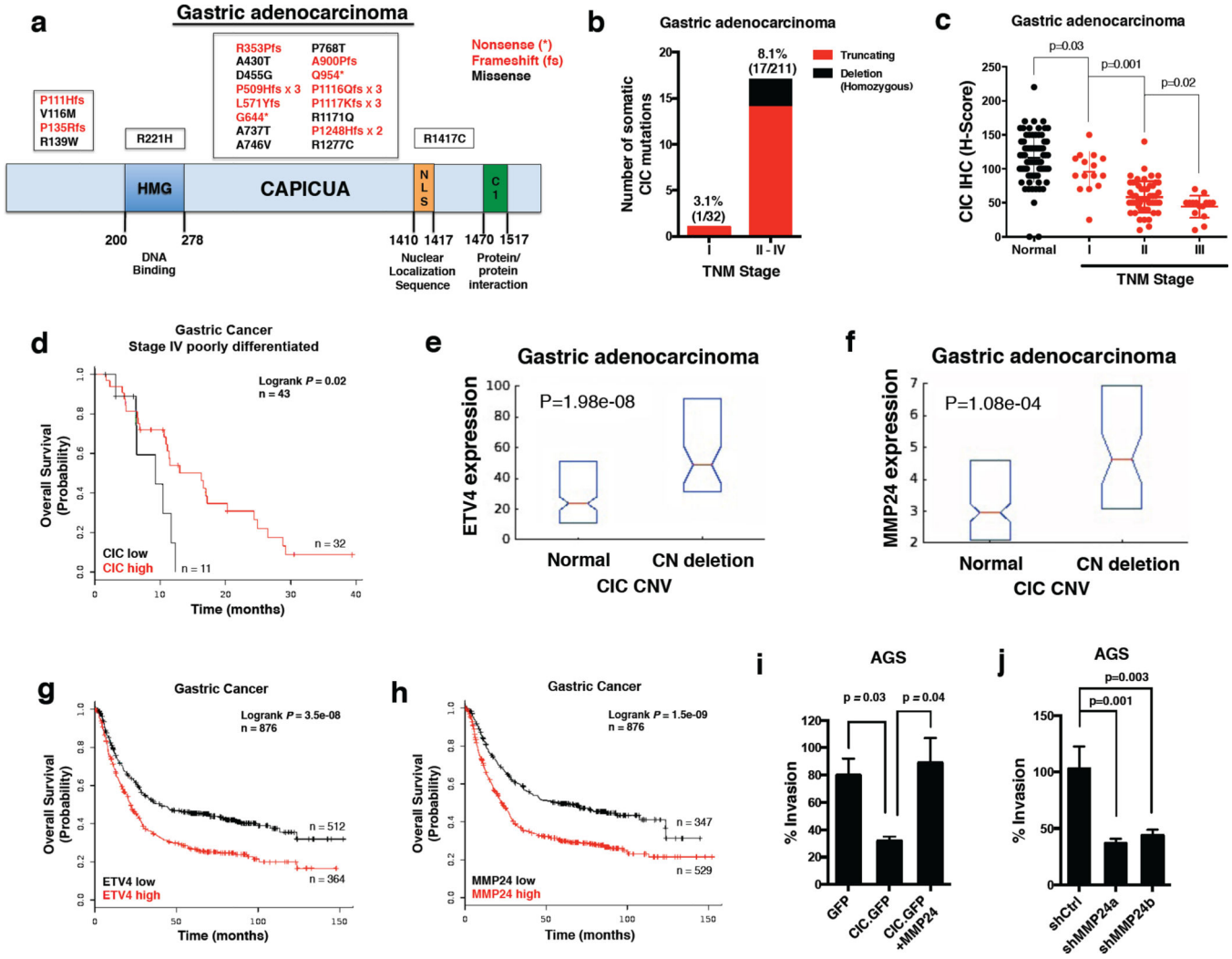

Figure 6. The CIC-ETV4-MMP24 metastatic axis is deregulated in gastric cancer

(a) CIC somatic mutations in TCGA GA specimens. (b) CIC deleterious mutations in GA stratified by TNM stage (243 out of 287 patients with clinical staging data available at the time of analysis). (c) Nuclear CIC expression in 84 human GA tissue specimens. Mean +/− SEM, 116 +/− 3.9 (normal, n=80), 95 +/− 7.5 (stage I, n=15), 58 +/− 3.1 (stage II, n=54), 44 +/− 4.1 (stage III, n=15). p-values, Student's t-test. (d) Overall survival (OS) for stage IV, poorly differentiated gastric cancer. n=43, p=0.02. *CIC* probe 212784_s_at. (e) Boxplots indicating median (red bar) and interquartile range (blue box) of *ETV4* mRNA expression levels in TCGA GA patient tumors with *CIC* copy number (CN) loss (p=1.98e-08, n=287). (f) Boxplots indicating mean (red bar) and interquartile range (blue box) of *MMP24* mRNA levels (RSEM) in TCGA GA patient tumors with *CIC* CN (p=1.08e-04, n=287). (g) OS in gastric cancer patients with either *ETV4* high or *ETV4* low mRNA expression. n=876, p=3.5e-08. *ETV4* probe 211603_s_at. (h) OS KM analysis in gastric cancer patients with either *MMP24* high or *MMP24* low mRNA expression. n=876, p = 1.5e-09. *MMP24* probe 213171_s_at. (i) Invasion of AGS cells with GFP control, CIC-GFP, or CIC-GFP with restored MMP24 expression (+MMP24). p-values, one-way ANOVA. Results of two

independent experiments in triplicate. Error bars represent SEM. (j) Invasion of AGS cells with shCtrl, shMMP24a, or shMMP24b. p-values, one-way ANOVA. Results of two independent experiments in triplicate.

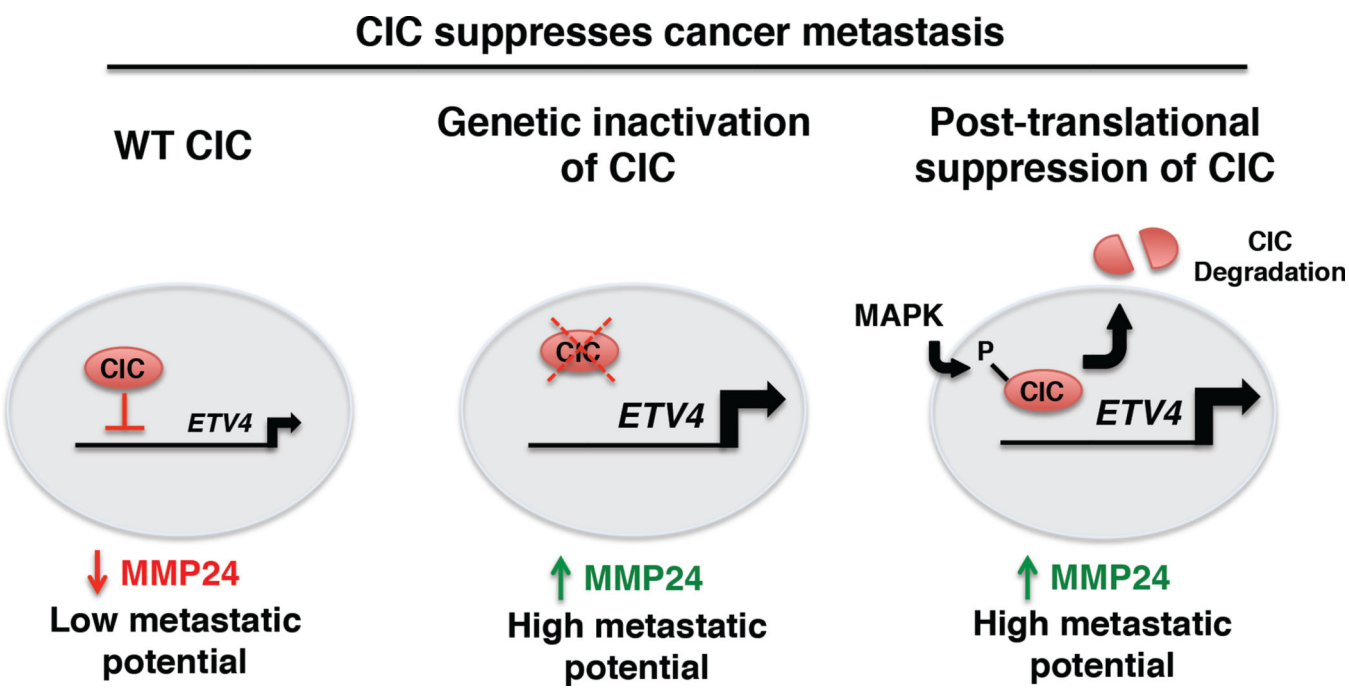

Figure 7. CIC suppresses cancer metastasis

Model of CIC mediated suppression of the ETV4-MMP24 pro-metastatic axis. De-repression of ETV4-MMP24 via genetic or functional (ERK-mediated post-translational) CIC suppression drives cancer metastasis.